Accepted Manuscript

Alteration of immature sedimentary rocks on Earth and Mars: Recording aqueous and surface-atmosphere processes

Kevin M. Cannon, John F. Mustard, Mark R. Salvatore

PII: S0012-821X(15)00095-3
DOI: http://dx.doi.org/10.1016/j.epsl.2015.02.017
Reference: EPSL 13103

To appear in: *Earth and Planetary Science Letters*

Received date: 7 July 2014
Revised date: 10 February 2015
Accepted date: 12 February 2015

Please cite this article in press as: Cannon, K.M., et al. Alteration of immature sedimentary rocks on Earth and Mars: Recording aqueous and surface-atmosphere processes. *Earth Planet. Sci. Lett.* (2015), http://dx.doi.org/10.1016/j.epsl.2015.02.017

Highlights

- We characterized alteration processes in the Carapace Sandstone from Antarctica
- A period of aqueous alteration is superimposed by a thick oxidation rind
- Similar alteration processes may be recorded in sedimentary rocks on Mars
- Sedimentary rocks may record alteration with greater fidelity than intact basalt

Alteration of immature sedimentary rocks on Earth and Mars: Recording aqueous and surface-atmosphere processes

Kevin M. Cannon[a,*], John F. Mustard[a], Mark R. Salvatore[b]

[a]Department of Earth, Environmental, and Planetary Sciences, Brown University
134 Brook Street, Box 1846, Providence RI 02912, USA
[b]School of Earth and Space Exploration, Arizona State University
PO Box 871404, Tempe AZ 85287-1404, USA
*To whom correspondence should be addressed.

Email for Kevin M. Cannon: kevin_cannon@brown.edu.
Phone for Kevin M. Cannon: (+1) 401-863-3485

Email for John F. Mustard: john_mustard@brown.edu.
Phone for John F. Mustard: (+1) 401-863-2417

Email for Mark R. Salvatore: msalvatore@asu.edu
Phone for Mark R. Salvatore: (+1) 480-727-2461

Abstract

Rock alteration and rind formation in analog environments like Antarctica may provide clues to rock alteration and therefore paleoclimates on Mars. Clastic sedimentary rocks derived from basaltic sources have been studied *in situ* by martian rovers and are likely abundant on the surface of Mars. However, how such rock types undergo alteration when exposed to different environmental conditions is poorly understood compared with alteration of intact basaltic flows. Here we characterize alteration in the chemically immature Carapace Sandstone from Antarctica, a terrestrial analog for martian sedimentary rocks. We employ a variety of measurements similar to those used on previous and current Mars missions. Laboratory techniques included bulk chemistry, powder X-ray diffraction (XRD), hyperspectral imaging and X-ray absorption spectroscopy. Through these methods we find that primary basaltic material in the Carapace Sandstone is pervasively altered to hydrated clay minerals and palagonite as a result of water-rock interaction. A thick orange rind is forming in current Antarctic conditions, superimposing this previous aqueous alteration signature. The rind exhibits a higher reflectance at visible-near infrared wavelengths than the rock interior, with an enhanced ferric absorption edge likely due to an increase in Fe^{3+} of existing phases or the formation of minor iron (oxy)hydroxides. This alteration sequence in the Carapace Sandstone results from decreased water-rock interaction over time, and weathering in a cold, dry environment, mimicking a similar transition early in martian history. This transition may be recorded in sedimentary rocks on Mars through a similar superimposition mechanism, capturing past climate changes at the hand sample scale. Our results also suggest that basalt-derived sediments could have sourced significant

volumes of hydrated minerals on early Mars due to their greater permeability compared with intact igneous rocks.

Keywords: Mars; sedimentary; weathering; alteration; spectroscopy

1.0 Introduction

Earth and Mars host extensive sedimentary strata that record the formation and subsequent alteration of their crusts. On Earth, sedimentary rocks can become highly processed and reach a state of chemical and mineralogical maturity as a result of sediment recycling. In contrast, martian counterparts may host more first-generation sediments due to lack of plate tectonics. It is important to understand how these martian sedimentary rocks record past surface and subsurface conditions in order to characterize ancient martian environments.

Mars' basaltic crust has been modestly altered through interaction with liquid water, and both remotely sensed data and rover observations suggest an evolution in the style and extent of this alteration through time (Bibring et al., 2005; Morris et al., 2006a,b; Mustard et al., 2008; Murchie et al., 2009). Bibring et al. (2006) define three 'eras' of different alteration styles in Mars history: an ancient clay-dominated era, a later sulfate-rich era, and the current era with anhydrous iron oxide formation. During the first two mineralogical eras – which may not actually be temporally distinct (Zolotov and Mironenko, 2014) – rocks in some regions were significantly altered in the presence of water; since then, physical erosion has dominated and chemical weathering on a global scale has been limited to slow anhydrous oxidation (Gooding et al., 1992; Burns and

70 Fisher, 1993; Goetz et al., 2005; Hurowitz and McLennan, 2007; McGlynn et al., 2012).
71 Transitions between these eras are not well understood, but the shifts likely involved
72 global changes (Bibring et al., 2006) and a “great drying” of the surface environment
73 (Kite et al., 2014). The rock record documents these changes, and understanding how it
74 does so is crucial to unraveling the geologic history of Mars (e.g., Grotzinger and
75 Milliken, 2012). It is also important to assess how different alteration styles may obscure
76 remote measurements of rock mineralogy and chemistry, for example through formation
77 of optically thick surficial rinds or coatings.

78 Sedimentary rocks on Mars, like those found in Terra Meridiani or Gale Crater
79 (McLennan et al., 2005; McLennan et al., 2014; Milliken et al., 2010; 2014), are likely
80 more reliable in recording post-depositional transitions in alteration regimes (i.e., aqueous
81 to cold and dry) than crystalline igneous rocks. These sedimentary rocks may be
82 chemically and mineralogically immature by terrestrial standards because the martian
83 basaltic crust differs fundamentally from Earth's more evolved tertiary crust (Taylor,
84 1989; Grotzinger et al., 2013; McLennan et al., 2014). Sediments on Mars are
85 presumably sourced from mafic-rich precursors resulting in enhanced olivine, pyroxene,
86 and calcic plagioclase (Vaniman et al., 2014) compared to quartzofeldspathic sediments
87 familiar in terrestrial settings. Thus from a thermodynamic standpoint martian
88 sedimentary rocks are much more susceptible to chemical alteration than typical
89 siliciclastic sediments on Earth (Goldich, 1938; Nesbitt and Wilson, 1992), and because
90 sedimentary rocks can exhibit significant porosity and permeability they should be
91 preferentially altered in comparison to intact crystalline basalt on Mars. Assuming the

availability of water, these features of immature sedimentary rocks enhance their fidelity in recording water-rock interactions and therefore past environmental conditions.

Because alteration products have been widely detected on the basaltic martian surface (Mustard et al., 2008; Carter et al., 2013), many authors have investigated chemical weathering of whole basaltic rocks under different alteration regimes. Studies at sites such as the Antarctic Dry Valleys (ADV) and Iceland (Allen and Conca, 1991; Bishop et al., 2002; Chevrier et al., 2006; Ehlmann et al., 2012: Salvatore et al., 2013a) have revealed largely intact basalts where alteration is restricted to thin surface rinds or fractures. No similar field studies have focused on clastic sedimentary rocks sourced from basaltic precursors, although Antarctic soils have received attention as Mars analogs (e.g., Bishop et al., 1996; Bishop et al., 2013). Thus it is poorly understood how Mars-like sedimentary rocks are altered under different environmental conditions and how they may record changes in those conditions. The objective of this work is to investigate a relevant analog material, the Carapace Sandstone from Carapace Nunatak in Antarctica, to determine its alteration history and the implications for the alteration of martian sedimentary rocks. We show that single hand samples of the Carapace Sandstone record multiple alteration regimes: a past subsurface water-rich environment and the current frigid desiccative Antarctic environment, similar to conditions that likely occurred on early Mars and those on Mars today.

2.0 Carapace Nunatak

The Carapace Sandstone is from Carapace Nunatak in Antarctica and is a relevant analog to martian sedimentary rocks because it is partly sourced from basaltic protolith,

and because of its original mineralogical and chemical immaturity as demonstrated below. Carapace Nunatak is located north of the ADV at 76°53'S, 159°25'E with a 1.6 km^2 exposed footprint above the ice. The extremely cold and dry climate in the Transantarctic Mountains provides the only terrestrial environment similar to martian conditions during the current Amazonian era (Marchant and Head, 2007). No location on Earth is a perfect analog for Mars, but cold Antarctic temperatures and lack of rainfall promote low-energy 'Amazonian-style' rock and soil alteration processes (Allen and Conca, 1991; Claridge and Campbell, 1984; Salvatore et al., 2013a,b) where chemical weathering is mostly cation-conservative and where poorly-crystalline alteration phases do not readily mature to fully crystalline clays and salts.

The 430 m stratigraphic section exposed at Carapace consists of the basal Jurassic-aged Carapace Sandstone (CS hereafter) conformably overlain by thick basaltic flows and hyaloclastite lenses of the Kirkpatrick Basalt (Figure 1; Gunn and Warren, 1962; Ballance and Watters, 1971; Ross, 2005). The CS is dated to ~177 Ma based on plant fossils (Balance and Watters, 2002) and is sourced partly from basaltic detritus. It is a cross-bedded lithic sandstone with coarser beds of conglomerate and finer beds of mudstone throughout its 130 m vertical extent. Ballance and Watters (1971) describe the depositional environment as: “shallow, north-east-flowing, ephemeral streams on a subsiding alluvial plain.” Several hand samples of the CS were collected in November 2011 by one of the authors. We used a representative sample, CN004, that was large enough for all for the analyses described herein. In the field, it was noted that broken rock surfaces exhibit centimeter-scale yellow-orange rinds (see Fig. 7) likely related to oxidative weathering processes explored below.

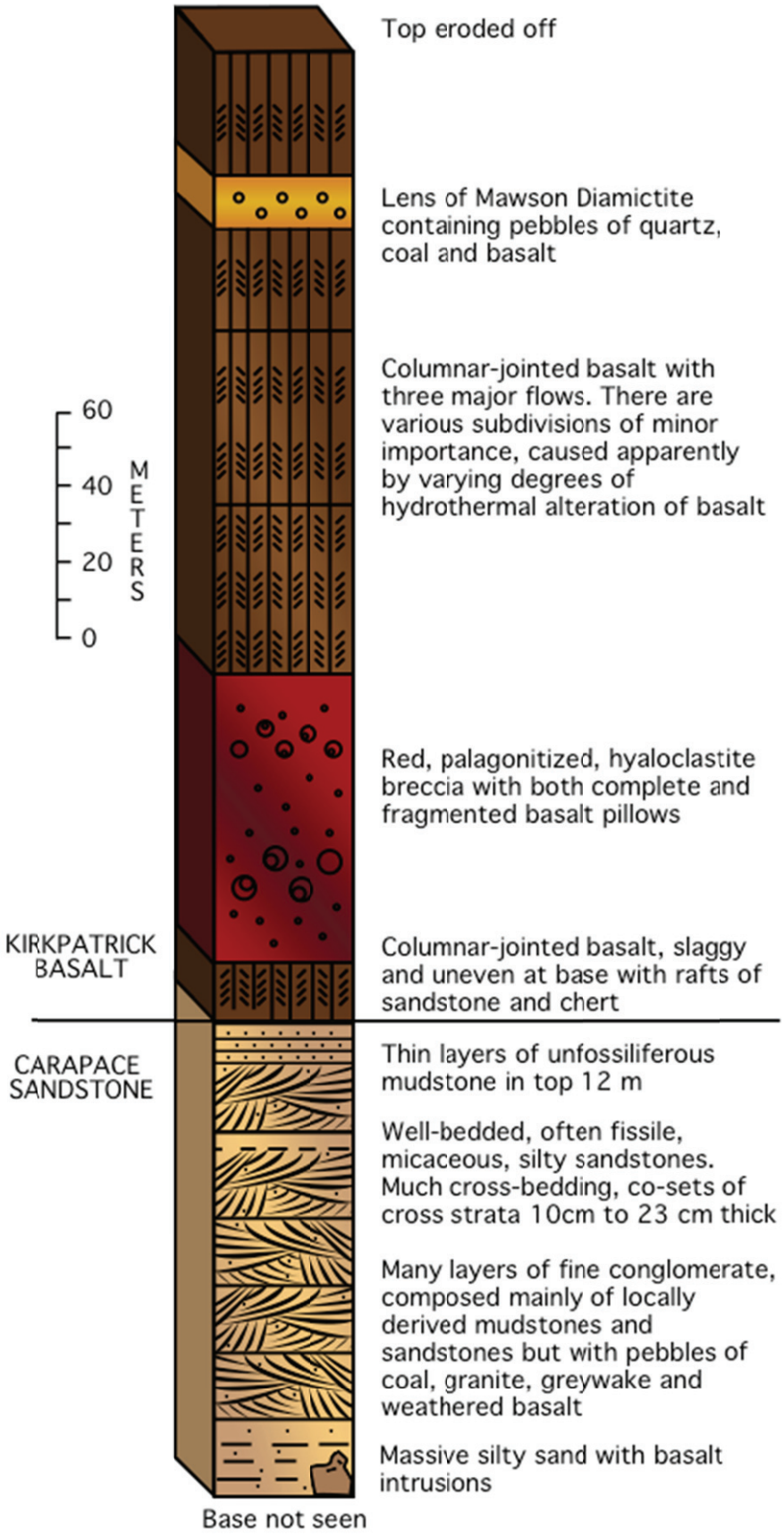
Top eroded off
Lens of Mawson Diamictite containing pebbles of quartz, coal and basalt
Columnar-jointed basalt with three major flows. There are various subdivisions of minor importance, caused apparently by varying degrees of hydrothermal alteration of basalt
60
40
20
0
METERS
Red, palagonitized, hyaloclastite breccia with both complete and fragmented basalt pillows
KIRKPATRICK BASALT
Columnar-jointed basalt, slaggy and uneven at base with rafts of sandstone and chert
CARAPACE SANDSTONE
Thin layers of unfossiliferous mudstone in top 12 m
Well-bedded, often fissile, micaceous, silty sandstones. Much cross-bedding, co-sets of cross strata 10cm to 23 cm thick
Many layers of fine conglomerate, composed mainly of locally derived mudstones and sandstones but with pebbles of coal, granite, greywake and weathered basalt
Massive silty sand with basalt intrusions
Base not seen

<Figure 1 location (1 column)>

Fig. 1. Generalized stratigraphic section of Carapace Nunatak. Hand samples were taken from within the crossbedded Carapace Sandstone. Redrawn from Figure 9 in Ballance and Watters (1971).

3.0 Materials and methods

We applied a variety of instrumental techniques to investigate the bulk properties of the CS and the expression of its alteration history. Most of these techniques are analogous to instruments utilized by past/current Mars missions, or that may be used in future missions (Table 1). In addition to these techniques we also used μXANES and μXRF synchrotron measurements to map chemistry and to determine Fe redox state, and we used scanning electron microscopy of thin sections for more detailed petrographic studies. Polished thin sections were prepared from hand samples of the CS and cut perpendicular to the exposed outer surface; this best exposes the transition from fresh interior to outer rind. We characterized the mineralogy, grain relationships and textures of these thin sections by investigating them with both reflected and transmitted light microscopy. The sections were also imaged in backscattered secondary electron (BSE) mode on a LEO 1530 scanning electron microscope (SEM) with an accelerating voltage of 20 keV and a working distance of 7 mm.

Table 1.

Instrumental techniques used in this study and analogous measurements made by Mars missions.

Instrumental technique	Analogous Mars instrument (mission)	Reference
Petrographic studies	Mars Hand Lens Imager (Mars Science Laboratory)	Edgett et al. (2012)
Visible near-infrared spectroscopy	Compact Reconnaissance Imager for Mars (Mars Reconnaissance Orbiter)	Murchie et al. (2007)
Hyperspectral imaging	Ultra Compact Imaging Spectrometer (possible future missions)	Van Gorp et al. (2014)
Bulk chemistry of major elements	Alpha Proton X-ray Spectrometer (Pathfinder, Mars Exploration Rover, Mars Science Laboratory)	Rieder et al. (1997)
Micro X-Ray absorption near edge spectroscopy	Mössbauer Spectrometer (Mars Exploration Rover)	Klingelhöfer et al. (2003)
Powder X-ray Diffraction	CheMin mineralogical instrument (Mars Science Laboratory)	Blake et al. (2012)

162

163

164 *3.1 Chemistry and mineralogy*

To determine chemical abundances of Si, Al, Ca, Fe, Mg, Mn, Ti, K, Na and P in the CS we used flux fusion followed by inductively coupled plasma-atomic emission spectrometry (ICP-AES) on separated powders from the rock rind and interior. Samples were prepared using the specific methods detailed in Murray et al. (2000) and run on a JY2000 Ultrace ICP-AES at Brown University. We ran samples in triplicate along with blanks (100% flux) and powder standards BCR-2 (Wilson, 1997a), BHVO-2 (Wilson, 1997b), MAG-1 (Flanagan, 1976), NIST SRM 1646a Estuarine Sediment, and NIST SRM 2711 Montana Soil in a randomized order. Elemental abundances (converted to wt. % oxide) were determined from linear regressions through the intensities of the reference standards after correcting for blanks and instrument drift.

To determine mineralogy of the samples we used X-ray diffraction (XRD) on similar crushed powders from the rind and interior of the CS with a Terra portable X-ray diffractometer. This instrument has a Cu-Kα radiation source, a 2θ range of 5-60° and a step size of 0.05°. 200 exposures were averaged from each sample to improve the signal to noise ratio. Phases were identified using peak-matching capabilities of the HighScore Plus software (PANalytical, vers. 2.0, 2011).

For elemental mapping and redox measurements the polished thin sections were analyzed using synchrotron-based micro-X-ray fluorescence (μXRF) and micro-X-ray absorption near edge structure (μXANES) techniques at the X26A beamline at the National Synchrotron Light Source facility. The beamline uses Rh-coated bent silicon mirrors in a Kirkpatrick-Baez geometry to focus a hard X-ray beam to a 5 μm (vertical) by 9 μm (horizontal) spot size. X-ray fluorescence was measured with a Canberra 9-element HPGe Array detector. μXRF elemental maps were made at an energy of 7.2 keV

188 through use of a motorized xy stage that rastered the sample in the beam path. μXANES
189 measurements were made by scanning over the Fe-Kα edge (7112 eV) for a large number
190 of points both in the exterior rind and fresh interior of the thin sections. We used a step
191 size of 0.2 eV for the pre-edge region (7100-7122 eV), with a coarser step size outside
192 this region. We ran standards of materials containing iron in various redox states and
193 coordination environments; these included Fe-metal foil, magnetite, hematite, fayalite,
194 nontronite, orthopyroxene and acmite. μXANES spectra were edge-step normalized using
195 the Athena software (Ravel, 2009). To isolate the pre-edge peak from the ascending
196 absorption edge we fitted the background with a 5th-order spline then subtracted it from
197 the original spectra, following the specific methods of Wilke et al. (2001).
198
199 *3.2 Spectroscopic techniques*
200 The orange rind on the CS is clearly visible to the naked eye and can be
201 characterized by reflectance spectroscopy at visible-near infrared (VNIR) wavelengths
202 (0.3-2.6 μm). Reflectance spectroscopy is also ideal for identifying hydrous minerals
203 such as clays, sulfates, or zeolites that may be present in the samples. This technique is
204 sensitive to electronic absorptions from crystal field transitions and charge transfers in
205 transition metals, particularly Fe (Burns, 1993), as well as molecular vibrational
206 absorptions from structural OH, H_2O and metal-OH groups in various minerals (Clark,
207 1999).
208 We used two spectroscopic approaches: high spectral resolution point
209 measurements of powders from both the rind and fresh interior of the CS, as well as
210 spatially resolved imaging spectroscopy of intact hand samples. Powders sieved to 63-

106 μm were measured at the Keck/NASA Reflectance Experiment Laboratory (RELAB) (Mustard and Pieters, 1987) at Brown University with a UV-Vis-NIR bidirectional reflectance (BDR) spectrometer from 0.3-2.6 μm with a 5 nm sampling interval. For spatially resolved spectroscopy we analyzed cut slabs of the CS at Headwall Photonics with high efficiency engineering models of VNIR and shortwave infrared (SWIR) imagers. The VNIR imager covers 0.4-1.0 μm with a 1.785 nm spectral resolution at up to 44 μm/pixel, and the SWIR imager covers 0.95-2.5 μm with 12.066 nm spectral resolution at up to 133 μm/pixel. We calibrated the images to relative reflectance using separate images of a Spectralon® white reference panel filling the frame with the same illumination conditions and viewing geometry as the samples. Dark current measurements were made by tightening the lens cap on the imagers during a reading and subtracting these values from the sample images.

4.0 Results

4.1 Petrographic observations

Microscope studies of thin sections support previous observations (Ballance and Watters, 1971; Ross, 2005) that the CS is both texturally and mineralogically immature compared to typical terrestrial siliciclastic rocks. It contains a significant fraction (>50% in some of our samples) of formerly glassy basaltic clasts that are now mostly altered to phyllosilicates and palagonite (Fig. 2). The term palagonite is contentious (Stroncik and Schmincke, 2002) but is used here to describe the non-crystalline orange-brown alteration product of volcanic glass. Angular grains of quartz, feldspar, detrital mica, coal, other light-toned lithic fragments, and irresolvable material compose the remainder of the rock.

The cement is mostly zeolite. The orange rind is not marked by any obvious textural or mineralogical boundary in thin section, even though a pronounced color boundary is visible to the naked eye in hand-samples. Similarly, there is no evidence for textural changes at the rind boundary in SEM images, and there is no presence of a coating as is typically seen in seen in desert varnish (Fig. 3) (e.g., Dorn, 2009). In other words, the orange rind has no obvious petrographic expression and cannot be linked to the presence of any mineral phase observable in thin section.

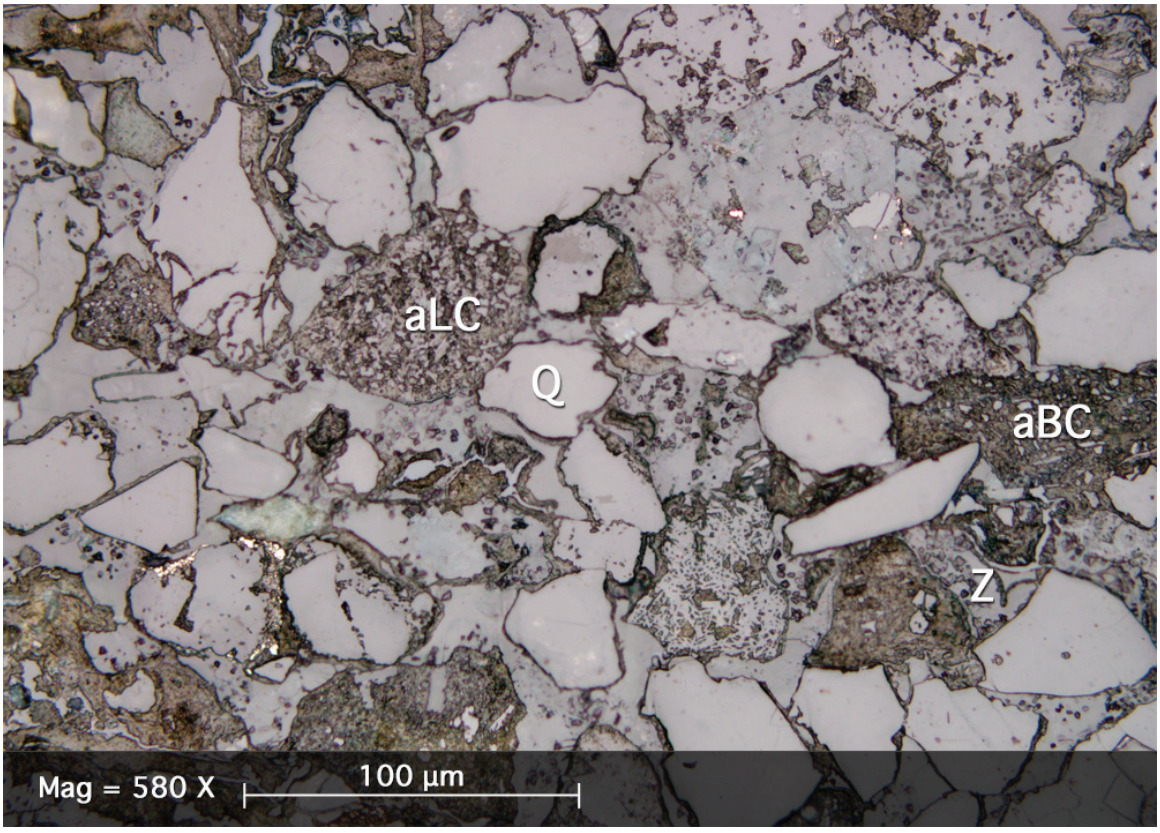

<Figure 2 location (1 column)>

Fig. 2. Optical reflected light micrograph of the Carapace Sandstone. Q = quartz, aLC = altered lithic clast, aBC = altered basaltic clast, Z = zeolite cement.

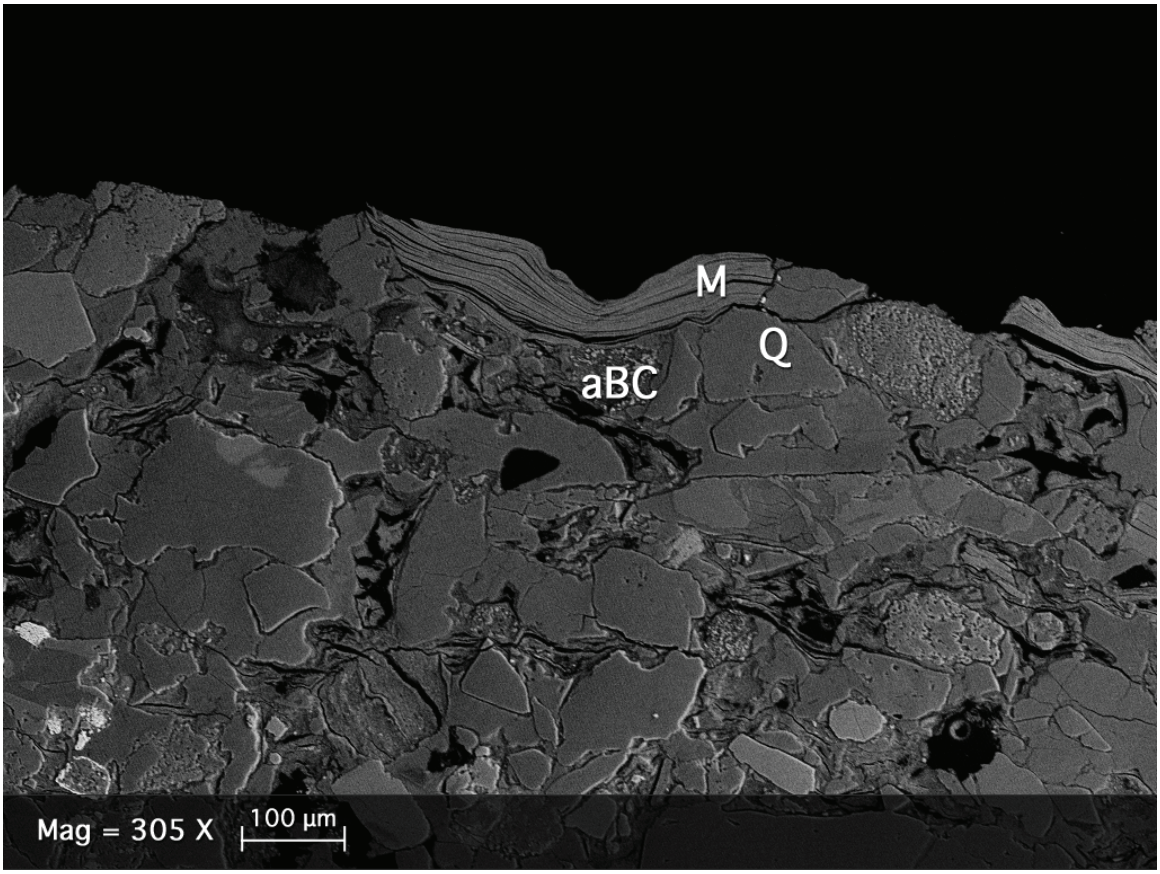

<Figure 3 location (1 column)>

Fig. 3. Backscatter secondary electron micrograph of the outer edge of the Carapace Sandstone containing the alteration rind. Q = quartz, M = detrital mica, aBC = altered basaltic clast. No presence of any coating is apparent.

4.2 Mineralogy and chemistry

X-ray diffraction analysis confirms the presence of clay minerals in the CS and shows evidence of poorly-crystalline phases (Fig. S1). Diffraction peaks were identified from quartz, clay minerals, pyroxene, sodic plagioclase, and zeolites (faujasite, among others). We attribute a strong peak at 5.95° 2θ (14.47 □) to the (001) reflection of one or more clay minerals, possibly partially hydrated smectites. Neither illite nor chlorite were

detected. There is a large, broad amorphous hump in the diffraction patterns caused by poorly crystalline or non-crystalline phases. It is unclear whether these phases are primary unaltered glass, gel-like weathering products such as palagonite, or both. The rind and interior of the sample do not differ significantly in their XRD patterns and no phases are uniquely present in one but not the other. Importantly, crystalline iron oxides such as hematite or goethite were not identified in XRD patterns of the rind.

In addition to being mineralogically immature, the CS is also chemically immature by terrestrial standards. Chemical Index of Alteration (CIA) is commonly used to quantify the degree of chemical weathering in sedimentary rocks (Nesbitt and Young, 1982) and is calculated as (Al_2O_3/(Al_2O_3+CaO+K_2O+Na_2O)) using molecular proportions. Fresh terrestrial basalts have CIA values of around 35-45, while highly mature altered sediments reach values upwards of 90 (Nesbitt and Young, 1982). The CS interior and exterior both have identical CIA values of 49. This suggests only a modest degree of chemical processing and a lack of extensive open-system leaching, in spite of the significant mineralogical changes caused by water-rock interaction. These values are consistent with other modern soils in the Antarctic Dry Valleys (Bishop et al., 2014).

Exterior and interior powders of the CS do not differ significantly in major elements (Table 2) and the low totals (~93%) are due to water and other volatiles, confirmed by loss on ignition measurements. The rind is not marked by a clear chemical boundary in μXRF chemical maps (Fig. 4) and there is no enrichment in Mn as is commonly observed in desert varnish. Chemical diffusion is not evident towards or away from the rind, although some potentially mobile elements like Mg were not mapped in the energy configuration used for the μXRF.

Table 2. Major ion chemistry (wt. % oxide) measured by ICP-AES for separated powders of the CS exterior (Ext) and interior (Int). All Fe is reported as FeO, and standard errors (SE) are derived from triplicate measurements.

Element	**Ext**	**Int**	**SE**
Al_2O_3	9.81	9.95	0.06
CaO	3.21	3.44	0.04
FeO	3.05	3.20	0.04
K_2O	1.58	1.63	0.02
MgO	2.07	2.10	0.02
MnO	0.04	0.05	0.0007
Na_2O	1.51	1.45	0.01
P_2O_5	0.04	0.05	0.004
SiO_2	71.98	71.05	0.5
TiO_2	0.46	0.47	0.01
Total	93.77	93.40	

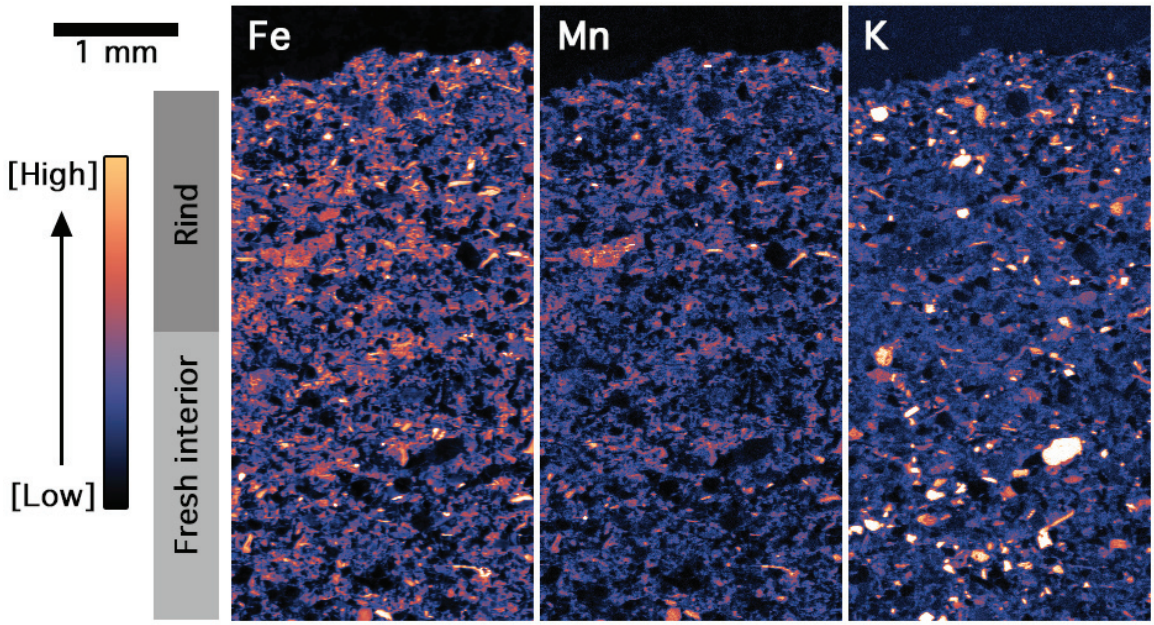

<Figure 4 location (2 columns)>

Fig. 4. μXRF chemical maps for Fe, Mn and K across the transition from exterior rind to fresh interior of the Carapace Sandstone. Relative concentrations are indicated by color. No obvious chemical boundary is present, and there is no evidence of chemical diffusion towards or away from the exterior surface of the rock.

Synchrotron μXANES spectra show that Fe is highly oxidized throughout the CS and that $Fe^{3+}/\Sigma Fe$ is slightly enhanced in the orange rind. White and McKinstry (1966) demonstrated that the Fe-Kα pre-edge peak centroid shifts systematically to higher energies for Fe^{3+} compared to Fe^{2+}, as is confirmed by our Fe-bearing standards (Fig. 5). Both the CS rind and interior have a much greater contribution from Fe^{3+} than Fe^{2+} in the pre-edge region, indicating that the rock is highly oxidized throughout. There is a modest difference in pre-edge centroid position between points measured from the interior and rind of the CS, with a tight cluster of exterior rind points at higher centroid energies. The

median relative centroid position is +2.13 eV for the interior and +2.17 eV for the rind, indicating an increase in Fe^{3+} in the exterior rind. This difference between the interior and exterior points is statistically significant at the 0.1 confidence level (Mann-Whitney U = 149.5, $n_1 = n_2 = 20$, P = 0.09 one-tailed), and is supported by the spectral evidence described below indicating an increase in Fe^{3+} in the rind.

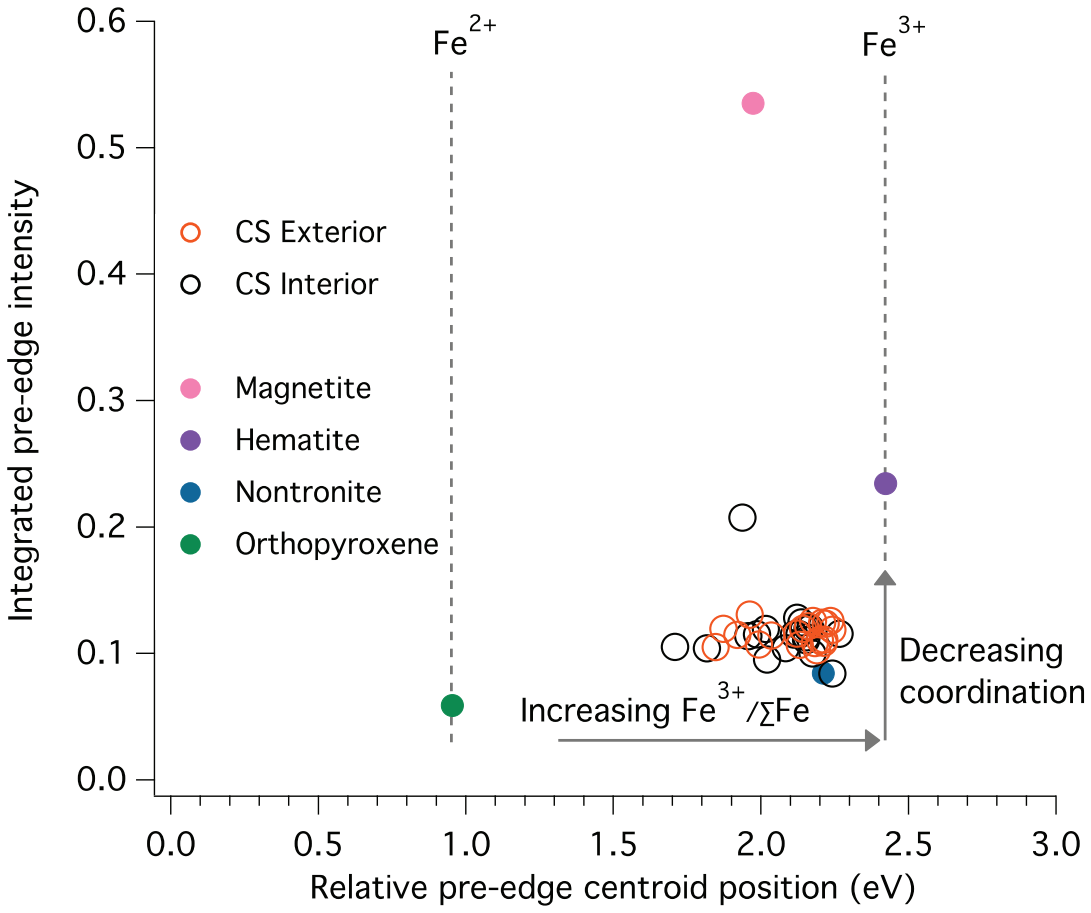

<Figure 5 location (1 column)>

Fig. 5. μXANES Fe pre-edge centroids and integrated intensities from clasts in the exterior and interior of the CS, compared to Fe-bearing standards run at the same

conditions. Centroids are shifted to higher energies with increasing Fe^{3+}, and integrated intensity increases as a function of decreasing coordination number.

4.3 Spectral signatures of alteration

Reflectance spectra of the interior of the CS differ from its orange-tinted rind as shown in Figure 6a. Crystal field (CF) absorptions from Fe^{3+} are present at 0.365, 0.425 and 0.495 μm in both exterior and interior, but the position of these absorptions does not uniquely identify any specific iron phases. These CF bands are superimposed on a sharp ferric absorption edge towards UV wavelengths caused by charge transfer absorptions between Fe^{2+}-Fe^{3+} and Fe^{3+}-O^{2-} (Hunt, 1977). The spectral slope from 0.55 to 0.8 μm is much steeper for the exterior rind compared to the interior, indicating a greater strength of this ferric edge and therefore a greater contribution from Fe^{3+}. The rind is brighter (higher reflectance values) than the fresh interior at all wavelengths, but especially so at wavelengths between 0.6 and 1.9 μm. Salvatore et al. (2013a) noted this brightness increase in similar rinds on the igneous Ferrar Dolerite from nearby Beacon Valley.

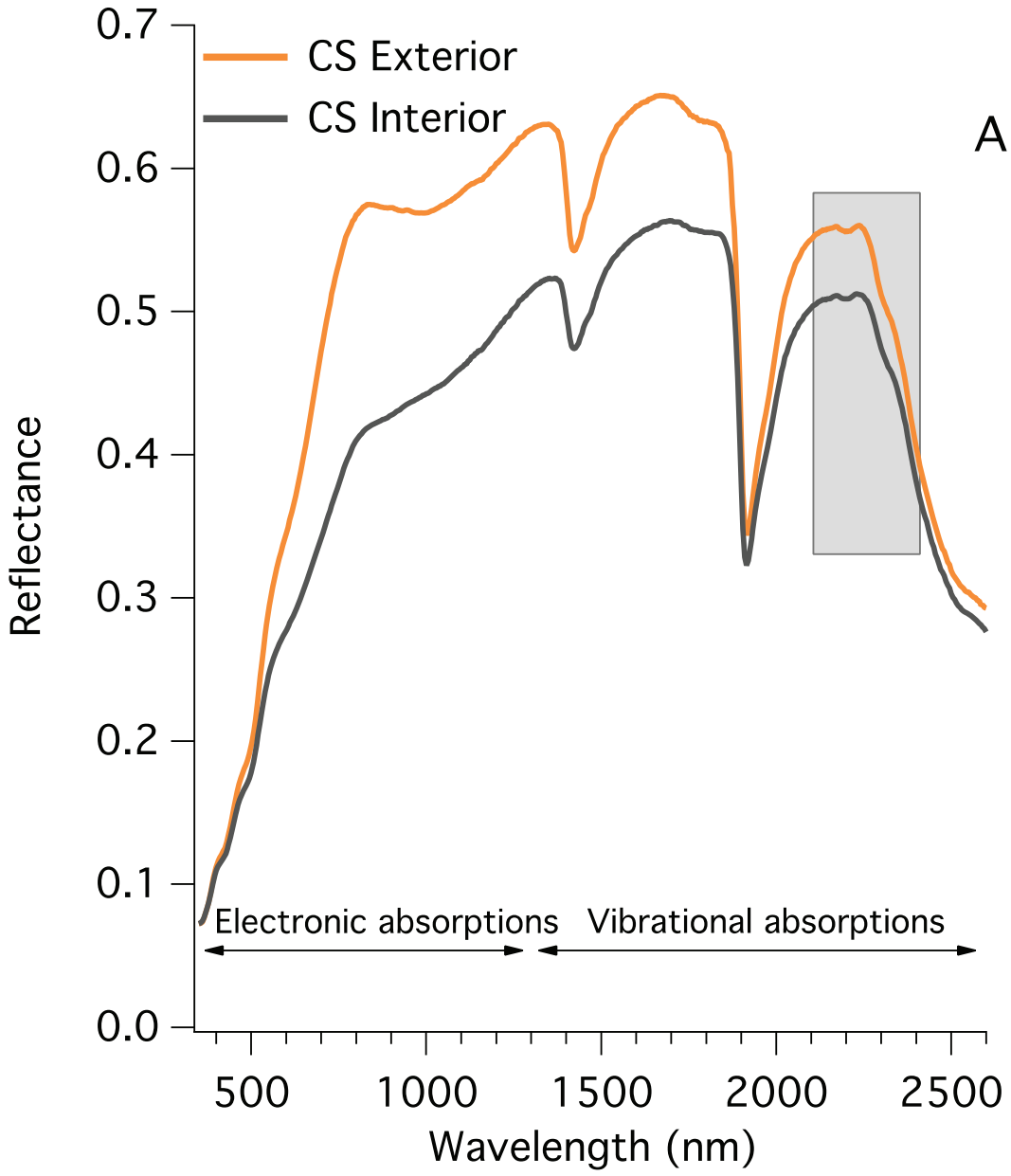
0.7
0.6
0.5
0.4
0.3
0.2
0.1
0.0
Reflectance
CS Exterior
CS Interior
A
Electronic absorptions
Vibrational absorptions
500
1000
1500
2000
2500
Wavelength (nm)

342

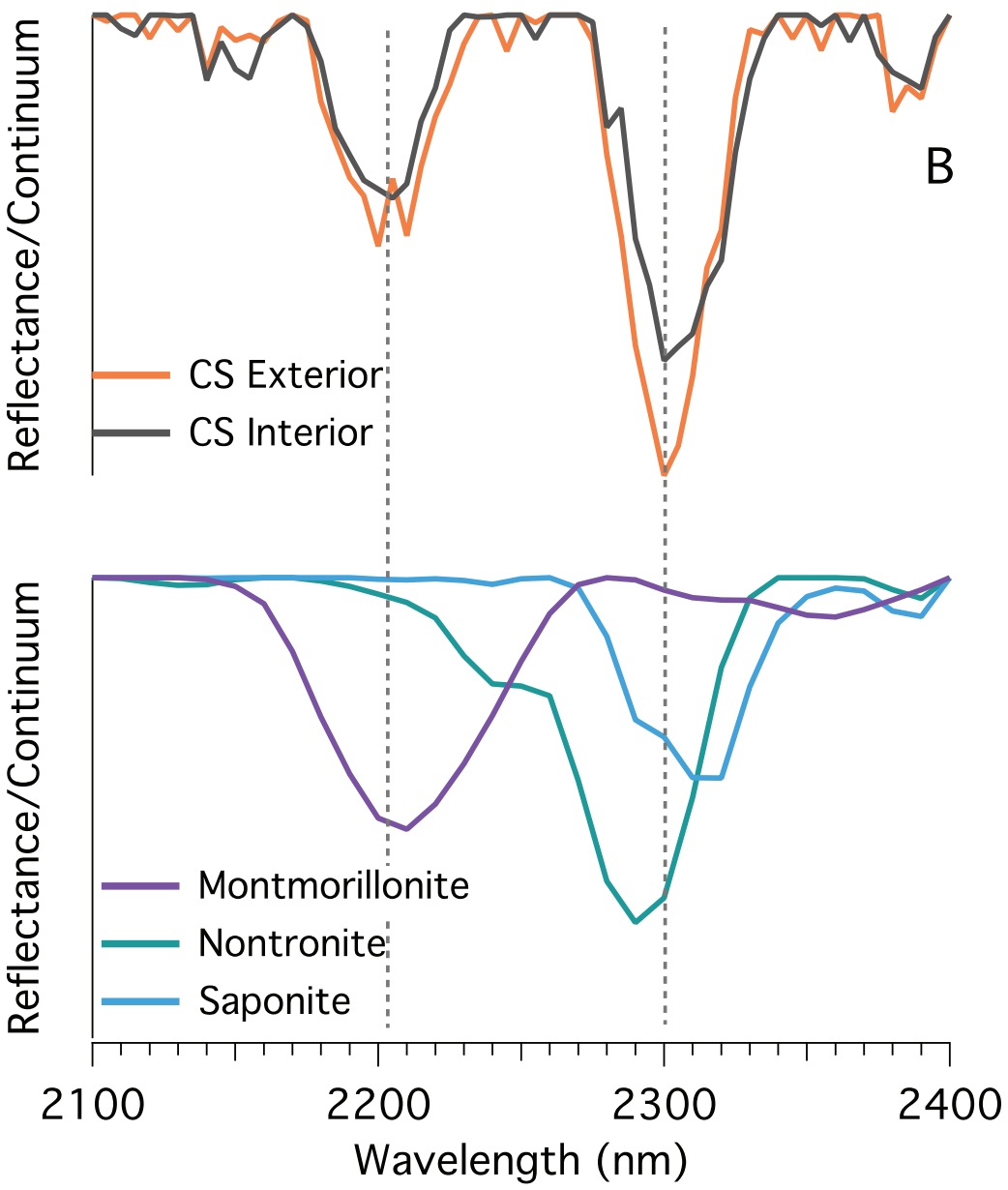

343

344 **<Figure 6 location (2 columns, A&B stacked horizontally)>**

345 **Fig. 6.** (a) VNIR reflectance spectra measured in RELAB for separated powders of the

346 Carapace Sandstone exterior (orange) and interior (gray) Shaded region shows subtle

347 absorptions from phyllosilicate minerals isolated in (b). (b) Zoom-in of (a) with a linear

348 continuum removed showing the characteristic metal-OH absorptions present in both the

CS rind and interior. Laboratory spectra of end-member montmorillonite (purple), nontronite (teal) and saponite (blue) are shown below for comparison.

The entire rock is highly hydrated but there is an increase in the band depth of H_2O-related absorptions in the rind of the CS compared to its interior. Absorptions at ~1.4 μm are caused by the first overtone of the OH^- stretching vibrations associated with structurally bound OH and H_2O. The depth of this absorption is calculated (equation 32 in Clark and Roush, 1984) as 0.136 for the rind and 0.103 for the interior, with a specific band minimum at 1.420 μm. The stronger absorption at 1.9 μm is a combination tone of the H_2O bending and stretching modes, indicating molecular water bound in a mineral structure, interlayer water in a clay structure, or adsorbed water (hydrogen bonded). Band depths for this absorption are 0.429 for the CS exterior and 0.399 for the interior, with a specific band minimum at 1.915 μm. This water may be adsorbed or bound in clay minerals, zeolites, amorphous phases or other hydrous minerals, but these cannot be uniquely distinguished based on the simple presence of water absorption features. However, two weak absorptions present in both exterior and interior separates at 2.205 μm and 2.300 μm could be caused by 2Al-OH and 2Fe/3Mg-OH combination overtones, respectively (Fig. 6b), with possible contribution from Si-OH bonds. These absorptions are common in hydrated silicate minerals such as phyllosilicates (e.g., Clark et al., 1990), and XRD results showed that clay minerals are present in the CS samples. Al-rich smectites (e.g., montmorillonite, beidellite) and/or allophane could contribute to the absorption at 2.205 μm, and Mg/Fe-rich smectites (e.g., saponite/nontronite), vermiculite, and/or carbonates likely cause the absorption at 2.300 μm. The specific position of this

longer wavelength absorption in the CS (2.300 μm, Fig. 6b) suggests a more magnesian composition in the Fe/Mg smectite solid solution series, if it is attributed to smectites alone (Clark et al., 1990).

Using hyperspectral imaging we mapped these electronic and vibrational absorption features across cut slabs of the CS. Figure 7a shows results from the VNIR hyperspectral imager in approximately true color, with the exterior rind clearly visible. In Figure 7b we map the value of the spectral slope from 0.5-0.8 μm, targeting the strength of the ferric absorption edge. A steeper slope in this spectral region corresponds to higher values (brighter) in this parameter map. The rind boundary is clearly visible in this representation and it crosscuts the angle of bedding in the sandstone, indicating this spectral difference cannot be attributed to some kind of depositional process or a different primary mineralogy where the rind is located. Figure 7c shows the strength of the 1.9 μm absorption feature as determined by the SWIR imager and represents a qualitative hydration map of the CS. The entire rock is highly hydrated, and observed metal-OH absorptions indicate that hydrous alteration phases are pervasive throughout the rind and interior. As is confirmed by point spectral measurements, the rind exhibits stronger H_2O absorptions relative to the interior.

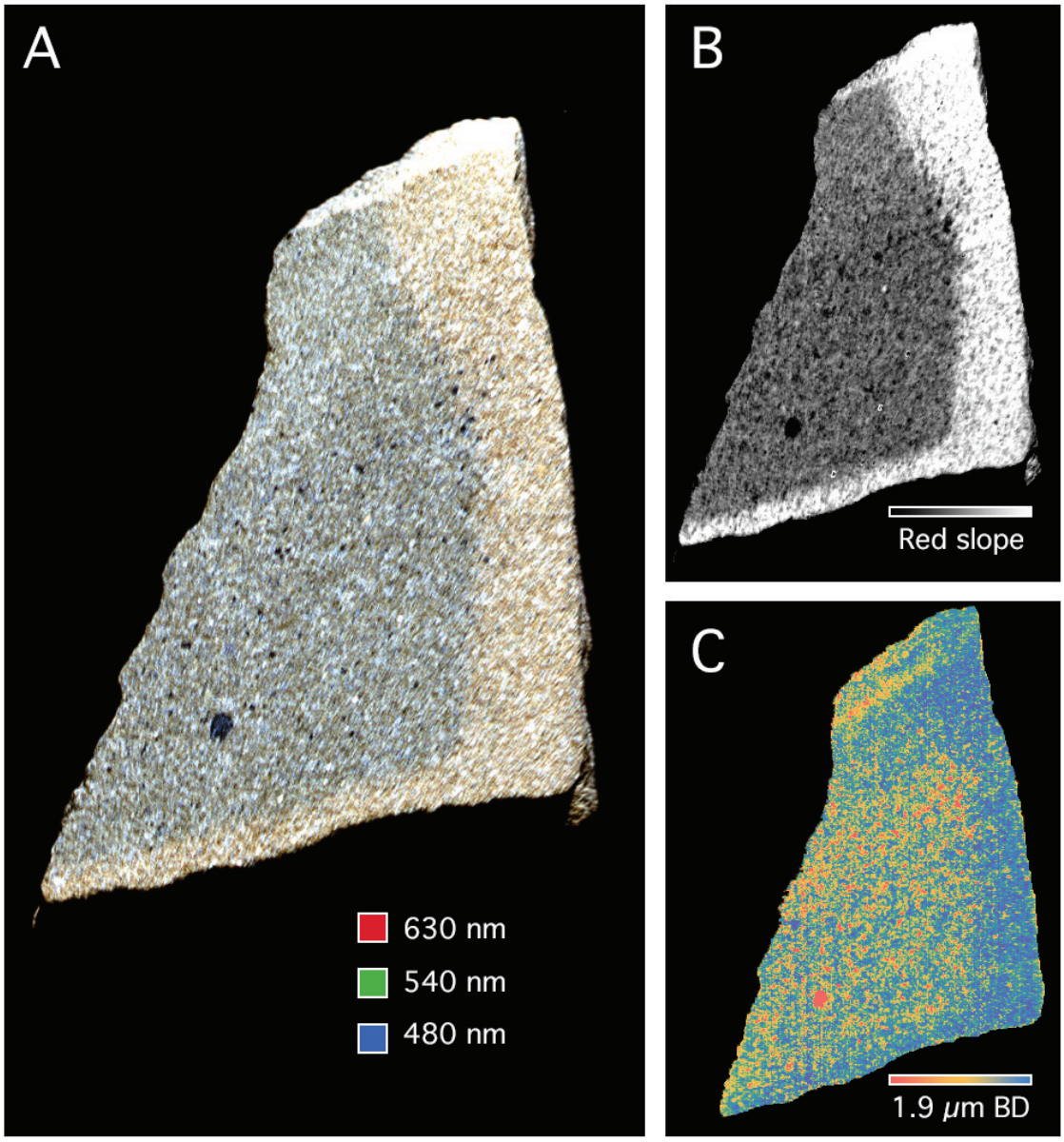

<Figure 7 location (2 columns)>

Fig. 7. (a) Hyperspectral VNIR image of a slab of the Carapace Sandstone in approximate true color, with the red channel at 630 μm, green at 540 μm and blue at 480 μm. Note the prominent orange appearance of the rind compared to the gray-blue fresh interior. (b) Spectral parameter map for the image in (a) showing the spectral slope from

0.5 to 0.7 μm. (c) Parameter map of the 1.9 μm absorption depth from the SWIR camera, where blue indicates higher hydration.

5.0 Discussion

5.1 Alteration regimes

The CS records two distinct alteration regimes: one dominated by aqueous alteration and the current one dominated by physical and oxidative weathering. Interactions with water altered the glassy mafic clasts to hydrated clays and palagonite throughout the entire rock; there is no increase in abundance of these phases in the exterior rind. It is unclear when the clay and palagonite formed relative to the zeolite cement, but Ballance and Watters (2002) suggest that interactions with hot groundwater at ~180 Ma, followed by burial beneath >1km of overlying basalt, led to multiple episodes of zeolite cementation at elevated temperatures (<240 °C). This shallow crustal setting is similar to environments proposed for hydrated silicate formation on early Mars (Ehlmann et al., 2011), and the lack of observed illite or chlorite implies the CS was not deeply buried for significant amounts of time (Hower et al., 1976; Chang et al., 1986). Aqueous alteration that transformed basaltic material in the CS likely took place syn- or post-depositionally. This is evidenced by the fact that original rounded glassy basaltic clast morphologies remain intact in the CS: previously altered clasts would not likely survive transportation without being broken up. Therefore we interpret the hydrated alteration minerals in the CS to be authigenic and not detrital.

Alteration characteristics of the CS fundamentally changed upon exposure to the current cold and dry Antarctic climate. This is expressed by the exterior rind that is not a

419 primary sedimentary feature, but instead is a superimposition formed in the cold and dry
420 environment at Carapace. Our field observations suggest rind formation weakens the
421 outer surface of the rock that flakes off, exposing fresh surfaces to further rind
422 development. We believe the rind–forming process is currently active, but cannot rule out
423 that it occurred in the past under different climate conditions. μXANES measurements
424 show a small increase in $Fe^{3+}/\Sigma Fe$ in this rind compared to inside the rock, but μXRF
425 mapping and SEM imaging show no obvious chemical boundary or coating. No
426 crystalline iron oxides were identified through XRD (sensitive to their presence at ~1%
427 levels), but the ferric absorption edge in VNIR spectra is greatly enhanced in the rind.
428 Taken together, we interpret these data to suggest either: (1) formation of small, nm- to
429 μm-scale, poorly crystalline iron (oxy)hydroxides that can contribute greatly to the
430 spectrum of the rock despite their minimal volumetric abundance (e.g., Morris et al.,
431 1993), and/or (2) a slight increase in the $Fe^{3+}/\Sigma Fe$ ratio of existing Fe-bearing phases.
432
433 *5.2 Rind formation process*
434 The rind on the CS is likely caused by atmospheric oxidation of Fe^{2+}, possibly
435 through a photochemical weathering process. Salvatore et al. (2013a,b) identified many
436 of the rind characteristics noted above in the Ferrar Dolerite of nearby Beacon Valley.
437 Those rocks are characterized by thin (<5 mm) bright orange-red rinds superimposed on a
438 fresh gray interior. The dolerite rinds dramatically change the spectral character of the
439 rock with no significant chemical or mineralogical changes across the boundary of the
440 rind. This suggests that rinds like the ones described here and by Salvatore et al.
441 (2013a,b) are common in low-energy weathering environments like Antarctica, regardless

442 of lithology. Salvatore et al. (2013a) suggest the dolerite rinds form through chemical
443 diffusion where electron holes (i.e., Fe^{3+}) migrate into the rock because of the redox
444 gradient between the rock interior and the atmosphere (Cooper et al., 1996). This model
445 could explain the rind on the CS, with the greater thickness of the CS rind caused by a
446 greater porosity and therefore deeper penetration of atmospheric oxygen. UV irradiation
447 might also be a cause of the iron oxidation, or enhance its rate. Huguenin (1974)
448 demonstrated that Fe-bearing silicates can be photooxidized by UV irradiation through
449 the general reaction $2FeO + ½O_2 + h\nu = Fe_2O_3$, and advocated that this process has been
450 important on the martian surface (Huguenin, 1976). These results were challenged
451 (Morris and Lauer, 1980), but defended by additional experiments (Huguenin, 1986).
452 Interestingly, Huguenin's experiments showed that intervals of adsorbed H_2O are
453 necessary for this photochemical weathering process to proceed, and in the case of the CS
454 this water could come from snowmelt, contact with ice/snow, and/or atmospheric water
455 vapor. The adsorbed H_2O causes Fe^{2+} to migrate to the rock/grain surface, sustaining the
456 oxidation process (Huguenin, 1974). Hydroxylation is a corollary of H_2O absorption to
457 mineral surfaces (e.g., Frederickson, 1951), which may explain why the CS rind is more
458 hydrated than the interior (Fig. 7). If photochemical weathering is a factor in these types
459 of colored rinds on Antarctic rocks, it warrants reappraising this potential process both on
460 Earth and Mars.
461
462 *5.3 Comparison with martian rover investigations*
463 The martian climate during the Amazonian era may cause similar oxidative rinds
464 in both sedimentary and igneous rocks (Salvatore et al., 2013a) that may have been

observed by *in situ* rover observations. The Mars Exploration Rover (MER) Opportunity explored sedimentary lithologies at Terra Meridiani, while the MER Spirit rover investigated mostly igneous lithologies at Gusev crater. Sedimentary bedrock at Meridiani (the Burns Formation) is interpreted as a reworked playa-type sulfate-bearing sandstone, with episodic post-depositional groundwater alteration (McLennan et al., 2005). Basaltic debris composes forty percent of the rock by mass (McLennan et al., 2005), and the presence of the hydrated Fe-sulfate jarosite (Klingelhöfer et al., 2004) points to acidic aqueous alteration of the sediments. Exposed and brushed surfaces of Meridiani sedimentary rocks differ significantly in their spectra from abraded targets, as shown by Pancam multispectral imaging (Figure 8). Specifically, the spectral slope at visible wavelengths increases for exterior surfaces, causing a buff tone. Dust might contribute to this coloration if it was not completely removed by the rover's brush, but a favored alternative explanation is the presence of a rind or coating (Knoll et al., 2008). Mössbauer data from the Gagarin rock target indicates statistically identical $Fe^{3+}/\Sigma Fe$ of 0.84±0.03 for both the brushed surface and the abraded rock, even though Pancam shows a greater ferric absorption edge for the exterior. An Antarctic-style oxidation rind is consistent with these data, and if present it superimposes the previous aqueous alteration at Meridiani. Similarly, igneous rocks at Gusev crater showed abnormally low compressive strengths (compared to expected values for basalt) when abraded by the rover (Thomson et al., 2014). These low strengths have been interpreted as evidence for weathering rinds several mm in thickness that do not have an obvious chemical signature (Thomson et al., 2014). Together the data from Opportunity and Spirit are consistent with

Antarctic-style rinds on both igneous and sedimentary martian rocks, but the evidence is inconclusive at present.

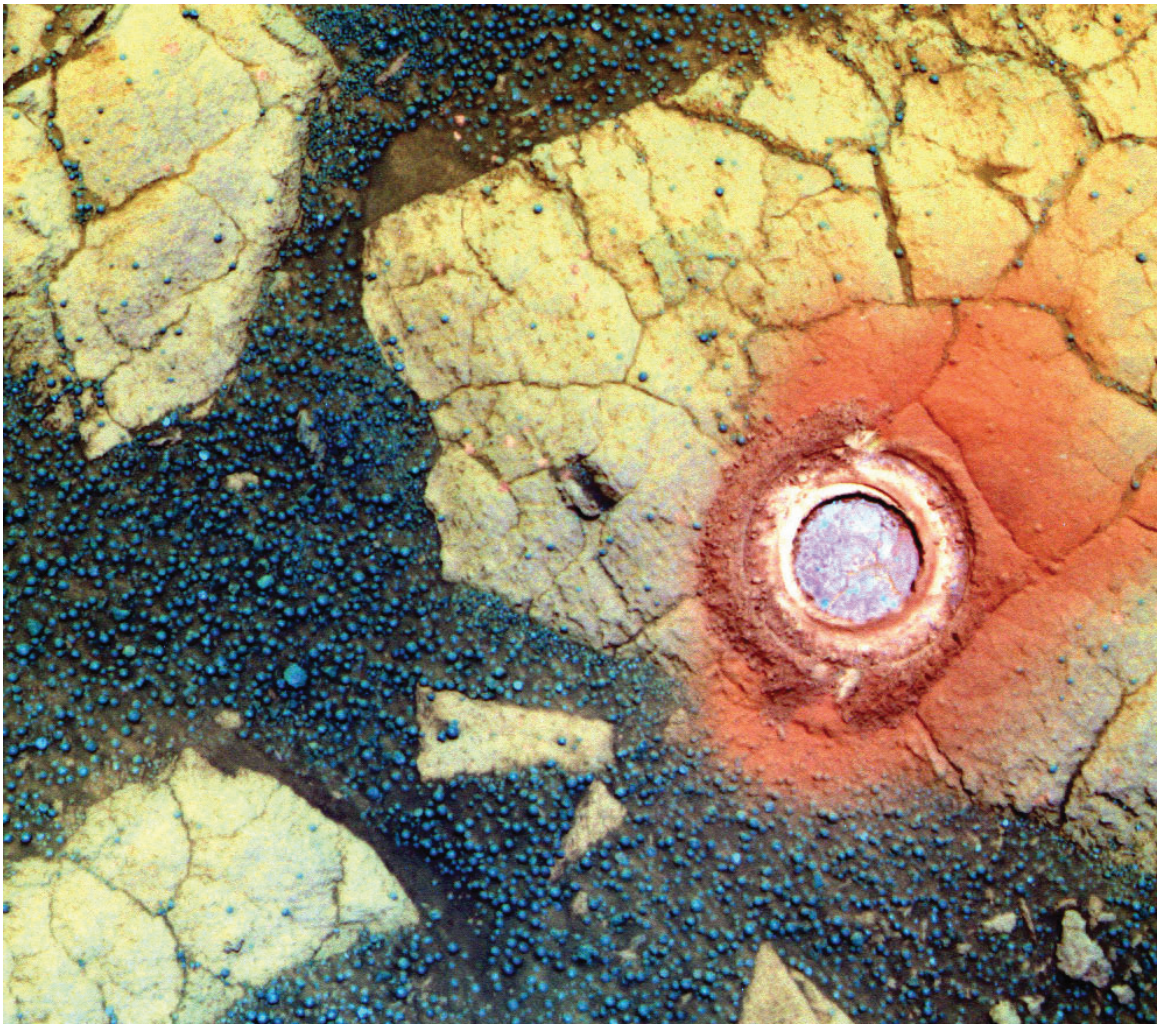

<Figure 8 location (1 column)>

Fig. 8. Pancam false-color multispectral image from the Gagarin target at Meridiani Planum. Red channel = 0.753 μm (L2), green channel = 0.535 μm (L5) and blue channel = 0.432 μm (L7). Image id:1P164134481IOF5000P2578. Image credit: Malin Space Science Systems/NASA JPL.

5.4 Implications for Mars

5.4.1 Recording past environments

Alteration sequences in the CS show that basaltic sedimentary rocks can serve as important records of past environmental conditions on Earth and Mars. Transitions between environments associated with the mineralogical 'eras' of Mars are typically imagined in terms of stratigraphic variations; mineral facies characteristic of a given era (e.g., Hesperian-aged sulfates) are deposited successively above those of the older ones (e.g., Noachian clays (Wiseman et al., 2008; Milliken et al., 2010)). The CS shows how these different alteration regimes (and thus past environments) could also be recorded through multiple alteration signatures progressively superimposed on one another within a single rock. The influence of the current Antarctic climate is recorded as an orange rind in the CS that does not destroy evidence for previous aqueous alteration at elevated temperatures. Sedimentary deposits at Meridiani Planum demonstrate a possible example of a similar change from a wetter to cold and dry environment recorded within a single stratigraphic unit.

5.4.2 Extent of alteration

Basaltic sedimentary rocks could have amplified the amount of aqueous alteration early in Mars' history. At low water to rock ratios whole basaltic flows are usually altered only in fractures or on contact surfaces (e.g., Ehlmann et al., 2012). In a sedimentary rock with modest porosity and permeability this alteration can be much more pervasive, as seen in the Carapace samples and suggested by early results from Gale Crater (Vaniman et al., 2014). On Mars there is an apparent discrepancy between the

extent of inferred aqueous alteration in the past (e.g., Carter et al., 2013) and climate models that fail to produce conditions warm and wet enough to account for that alteration (e.g., Mischna et al., 2013). This discrepancy may be biased by previous field studies of whole basalts on Earth where aqueous alteration is usually modest in volumetric extent and is limited by the creation of secondary porosity (Navarre-Sitchler et al., 2009). We suggest that less extensive aqueous alteration is required on Mars if some amount of hydrous alteration minerals were formed in porous siliclastic rocks rather than in intact basaltic flows. The importance of these basaltic sedimentary rocks in martian history has been relatively underappreciated until recently (Malin and Edgett, 2000; Grotzinger and Milliken, 2012).

6.0 Conclusions

Through a detailed study of the Carapace Sandstone from Antarctia we have demonstrated the importance of immature sedimentary rocks in deciphering the alteration history of Mars. Aqueous alteration in massive basalts is mostly limited to thin surficial coatings and fractures, while a sedimentary rock of the same composition can be pervasively altered in similar conditions. The Carapace Sandstone's secondary mineral assemblage consists of hydrated clay minerals and palagonite formed by pervasive water-rock interactions in the shallow subsurface. This alteration signature is superimposed by an orange rind caused by oxidation of Fe, likely forming in the current cryodesiccative Antarctic environment. Similar alteration profiles may be a common product of the Amazonian era on Mars and can aid in understanding when and how Mars dried out, if properly recognized. Products of successive alteration regimes on Mars may not simply

be laid down on top of each other in a layer-cake stratigraphy, and instead these transitions may cause superimposed records of alteration captured in a single rock.

Acknowledgements

We are greatly indebted to Ralph Milliken for suggestions that significantly improved this manuscript, and to Janice Bishop and an anonymous reviewer for thorough reviews. We would also like to thank Janette Wilson, Kwok Wong, Jennifer Bentz, Takahiro Hiroi, Joseph Bosenberg, Sue Wirick, and William Rao for assistance with instrumental techniques.. Portions of this work were performed at Beamline X26A, National Synchrotron Light Source (NSLS), Brookhaven National Laboratory. X26A is supported by the Department of Energy (DOE) - Geosciences (DE-FG02-92ER14244 to The University of Chicago - CARS). Use of the NSLS was supported by DOE under Contract No. DE-AC02-98CH10886.

References

Allen, C.C., Conca, J.L., 1991. Weathering of Basaltic Rocks Under Cold, Arid Conditions: Antarctica and Mars, Proc. Lunar Planet. Sci. 21, 711-717.

Ballance, P.F., Watters, W.A., 1971. The Mawson Diamictite and the Carapace Sandstone, formations of the Ferrar Group at Allan Hills and Carapace Nunatak, Victoria Land, Antarctica, New Zealand. J. Geo. Geophys. 14, 512-527, doi:10.1080/00288306.1971.10421945.

566 Ballance, P.F., Watters, W.A., 2002. Hydrothermal alteration, contact metamorphism,
567 and authigenesis in Ferrar Supergroup and Beacon Supergroup rocks, Carapace Nunatak,
568 Allan Hills, and Coombs Hills, Victoria Land, Antarctica. New Zealand J. Geo. Geophys.
569 45, 71-84, doi:10.1080/00288306.2002.9514960.
570
571 Bibring, J.-P., et al., 2005. Mars Surface Diversity as Revealed by the OMEGA/Mars
572 Express Observations. Science 307, 1576, doi:10.1126/science.1108806.
573
574 Bibring, J.-P., et al., 2006. Global Mineralogical and Aqueous Mars History Derived
575 from OMEGA/Mars Express Data. Science 312, 400, doi:10.1126/science.1122659.
576
577 Bishop, J.L., Koeberl, C., Kralik, C., Froeschl, H., Englert, P.A.J., Andersen, D.W.,
578 Pieters, C.M., Wharton, R.A., 1996. Reflectance spectroscopy and geochemical analyses
579 of Lake Hoare sediments, Antarctica. Geochimica Cosmochimica Acta 60, 765-785. doi:
580 10.1016/0016-7037(95)00432-7.
581
582 Bishop, J.L., Schiffman, P., Southard, R.J., 2002. Geochemical and mineralogical
583 analyses of palagonitic tuffs and altered rinds of pillow lavas on Iceland and applications
584 to Mars. Pp. 371-392 in: Volcano-Ice Interactions on Earth and Mars (J.L. Smellie &
585 M.G. Chapman, editors). Geological Society, Special Publication No.202, London.
586

587 Bishop, J.L., et al., 2013. Coordinated analyses of Antarctic sediments as Mars analog
588 materials using reflectance spectroscopy and current flight-like instruments for CheMin,
589 SAM and MOMA. Icarus 224, 309-325. doi: 10.1016/j.icarus.2012.05.014.
590
591 Bishop, J.L., Englert, P.A.J., Patel, S., Tirsch, D., Roy, A.J., Koeberl, C., Böttger, U.,
592 Hanke, F., Jaumann, R., 2014. Mineralogical analyses of surface sediments in the
593 Antarctic Dry Valleys: Coordinated analyses of Raman spectra, reflectance spectra and
594 elemental abundances. Phil. Trans. R. Soc. A 372, 20140198. doi:
595 10.1098/rsta.2014.0198.
596
597 Blake, D. et al., 2012. Characterization and Calibration of the CheMin Mineralogical
598 Instrument on Mars Science Laboratory. Space Sci. Rev. 170, 341-399,
599 doi:10.1007/s11214-012-9905-1
600
601 Burns, R.G., 1993. Mineralogical Applications of Crystal Field Theory. Cambridge
602 University Press, Cambridge, UK.
603
604 Burns, R.G., Fisher, D.S., 1993. Rates of Oxidative Weathering on the Surface of Mars. J.
605 Geophys. Res. 98, 3365-3372, doi:10.1029/92JE02055
606
607 Carter, J., Poulet, F., Bibring, J.-P., Mangold, N., Murchie, S., 2013. Hydrous minerals on
608 Mars as seen by the CRISM and OMEGA imaging spectrometers: Updated global view.
609 J. Geophys. Res. Planets 118, 831–858, doi:10.1029/2012JE004145.

610

611 Chang, H.K., Mackenzie, F.T., Schoonmaker, J., 1986. Comparisons between the
612 diagenesis of dioctahedral and trioctahedral smectite, Brazilian offshore basins, Clays and
613 Clay Minerals 34, 407-423.

614

615 Chevrier, V., Mathé, P.-E., Rochette, P., Gunnlaugsson, H.P., 2006. Magnetic study of an
616 Antarctic weathering profile on basalt: Implications for recent weathering on Mars. Earth
617 Planet. Sci. Lett. 244, 501-514, doi:10.1016/j.epsl.2006.02.033.
618 Claridge, G.G.C., Campbell, I.B., 1984. Mineral transformation during the weathering of
619 dolerite under cold arid conditions in Antarctica. New Zealand Journal of Geology and
620 Geophysics 27, 537-545.

621

622 Clark, R.N., 1999. Spectroscopy of rocks and minerals and principles of spectroscopy, in:
623 Rencz, A.N. (Ed.), Manual of Remote Sensing. John Wiley, New York, pp. 3–58.

624

625 Clark, R.N., Roush, T.L., 1984. Reflectance spectroscopy: Quantitative analysis
626 techniques for remote sensing applications. J. Geophys. Res. 89, 6329–6340,
627 doi:10.1029/JB089iB07p06329.

628

629 Clark, R.N., King, T.V.V., Klejwa, M., Swayze, G.A., 1990. High Spectral Resolution
630 Reflectance Spectroscopy of Minerals. J. Geophys. Res. 95, 12653-12680,
631 doi:10.1029/JB095iB08p12653.

632

633 Cooper, R.F., Fanselow, J.B., Poker, D.B., 1996. The mechanism of oxidation of a
634 basaltic glass: Chemical diffusion of network-modifying cations. Geochimica et
635 Cosmochimica Acta 60, 3253-3265, doi: 10.1016/0016-7037(96)00160-3.
636
637 Dorn, R.I., 2009. Desert Rock Coatings, in: Parsons, A.J., Abrahams, A.D. (Eds.)
638 Geomorphology of Desert Environments, 2nd ed. Springer, pp.153-186, doi:10.1007/978-
639 1-4020-5719-9_7.
640
641 Edgett, K.S. et al., 2012. Curiosity's Mars Hand Lens Imager (MAHLI) Investigation.
642 Space Sci. Rev. 170, 259-317.
643
644 Ehlmann, B.L. et al. 2011. Subsurface water and clay mineral formation during the early
645 history of Mars. Nature 479, 53, doi:10.1038/nature10582.
646
647 Ehlmann, B.L., Bish, D.L., Ruff, S., Mustard, J.F., 2012. Mineralogy and chemistry of
648 altered Icelandic basalts: application to clay mineral detection and understanding aqueous
649 environments on Mars. J. Geophys. Res. 117, E00J16, doi:10.1029/2012JE004156.
650
651 Flanagan, F.J., 1976. Descriptions and Analyses of Eight New USGS Rock Standards.
652 U.S. Geological Survey Professional Paper 840, 192 p.
653
654 Frederickson, A.F., 1951. Mechanism of Weathering. Geological Society of America
655 Bulletin 62, 221-232, doi:10.1130/0016-7606(1951)62[221:MOW]2.0.CO;2.

656

657 Goetz, W. et al. 2005. Indication of drier periods on Mars from the chemistry and

658 mineralogy of atmospheric dust. Nature 436, 62-65, doi:10.1038/nature03807.

659

660 Goldich, S.S., 1938. A Study in Rock-Weathering. J. Geol. 46(1), 17-58.

661

662 Gooding, J.L., 1992. Soil Mineralogy and Chemistry on Mars; Possible Clues from Salts

663 and Clays in SNC Meteorites. Icarus 99, 28-41, doi:10.1016/0019-1035(92)90168-7

664

665 Grotzinger, J.P., Milliken, R.E., 2012. The sedimentary rock record of Mars: distribution,

666 origins, and global stratigraphy, in Grotzinger, J.P. (Ed.) Sedimentary Geology of Mars.

667 SEPM Special Publication #102, pp. 1-48.

668

669 Grotzinger, J.P., Hayes, A.G., Lamb, M.P., McLennan, S.M., 2013. Sedimentary

670 Processes on Earth, Mars, Titan and Venus, in Mackwell, S.J. et al. (Eds.) Comparative

671 Climatology of Terrestrial Planets. Univ. of Arizona Press, Tucson, in press.

672

673 Gunn, B.M., Warren, G., 1962. Geology of Victoria Land between the Mawson and

674 Mulock Glaciers, Antarctica. N.Z. Geol. Surv. Bull. 71.

675

676 Hower, J., Eslinger, E.V., Hower, M.E., Perry, A., 1976. Mechanism of burial

677 metamorphism of argillaceous sediment: 1. Mineralogical and chemical evidence. GSA

678 Bulletin 87, 725-737.

679

680 Huguenin, R.L., 1974. The Formation of Goethite and Hydrated Clay Minerals on Mars.
681 J. Geophys. Res. 79, 3895-3905, doi:10.1029/JB079i026p03895.
682

683 Huguenin, R.L., 1976. Mars: Chemical weathering as a massive volatile sink. Icarus
684 28(2), 203-212, doi:10.1016/0019-1035(76)90033-6.
685

686 Huguenin, R.L., 1986. Photochemical Weathering and Contemporary Volatile Loss on
687 Mars. In: 17th Lunar Planetary Science Conference. Abstract #1189.
688

689 Hunt, G.R., 1977. Spectral Signatures of Particulate Minerals in the Visible and Near
690 Infrared. Geophysics 42, 501-513, doi:10.1190/1.1440721.
691

692 Hurowitz, J.A., McLennan, S.M., 2007. A ~3.5 Ga record of water-limited, acidic
693 weathering conditions on Mars. Earth Planet. Sci. Lett. 260, 432-443.
694

695 Kite, E.S., Lucas, A., Armstrong, J.C., Aharonson, O., Lamb, M.P., 2014. Resolving the
696 Great Drying of Mars: Paleo-Climate Versus Time from River Deposits in Aeolis Dorsa.
697 In: 45th Lunar and Planetary Science Conference, Abstract #1777.
698

699 Klingelhöfer, G. et al., 2003. Athena MIMOS II Mössbauer spectrometer investigation. J.
700 Geophys. Res. 108, E12, 8067. doi: 10.1029/2003JE002138.
701

Klingelhöfer, G. et al., 2004. Jarosite and Hematite at Meridiani Planum from Opportunity's Mössbauer Spectrometer. Science 306, 1740-1745, doi:10.1126/science.1104653.

Knoll, A.H. et al., 2008. Veneers, rinds, and fracture fills: Relatively late alteration of sedimentary rocks at Meridiani Planum, Mars. J. Geophys. Res. 113, E06S16. doi:10.1029/2007JE002949.

Malin, M.C., Edgett, K.S., 2000. Sedimentary Rocks of Early Mars. Science 290, 1927-1937, doi:10.1126/science.290.5498.1927 .

Marchant, D.R., Head III, J.W., 2007. Antarctic dry valleys: Microclimate zonation, variable geomorphic processes, and implications for assessing climate change on Mars. Icarus 192, 187-222, doi:10.1016/j.icarus.2007.06.018.

McGlynn, I.O., Fedo, C.M., McSween Jr., H.Y., 2012. Soil mineralogy at the Mars Exploration Rover landing sites: An assessment of the competing roles of physical sorting and chemical weathering. J. Geophys. Res. 117, E01006, doi:10.1029/2011JE003861.

McLennan, S.M. et al., 2005. Provenance and diagenesis of the evaporite-bearing Burns formation, Meridiani Planum, Mars. Earth Planetary Sci. Lett. 240, 95-121, doi:10.1016/j.epsl.2005.09.041.

McLennan, S.M. et al., 2014. Elemental Geochemistry of Sedimentary Rocks at Yellowknife Bay, Gale Crater, Mars. Science 343, 6169, doi:10.1126/science.1244734.

Milliken, R.E., Grotzinger, J.P., Thomson, B.J., 2010. Paleoclimate of Mars as captured by the stratigraphic record in Gale Crater. Geophys. Res. Lett. 37, L04201, doi:10.1029/2009GL041870.

Milliken, R.E., Ewing, R.C., Fischer, W.W., Hurowitz, J., 2014. Wind-blown sandstones cemented by sulfate and clay minerals in Gale Crater, Mars. Geophys. Res. Lett. 41, 1149–1154, doi:10.1002/2013GL059097.

Mischna, M.A., Baker, V., Milliken, R., Richardson, M., Lee, C., 2013. Effects of obliquity and water vapor/trace gas greenhouses in the early martian climate. J. Geophys. Res. 118, 560-576, doi:10.1002/jgre.20054.

Morris, R.V., Lauer Jr., H.V., 1980. The case against UV photostimulated oxidation of magnetite. J. Geophys. Res. 7, 605-608, doi:10.1029/GL007i008p00605.

Morris, R.V., Golden, D.C., Bell III, J.F., Lauer Jr., H.V., Adams, J.B., 1993. Pigmenting agents in Martian soils: Inferences from spectral, Mössbauer, and magnetic properties of nanophase and other iron oxides in Hawaiian palagonitic soil PN-9. Geochim. Cosmochim. Acta 57, 4597–4609, doi:10.1016/0016-7037(93)90185-Y.

748

749 Morris, R.V. et al., 2006a, Mössbauer mineralogy of rock, soil, and dust at Gusev crater,
750 Mars: Spirit's journey through weakly altered olivine basalt on the plains and pervasively
751 altered basalt in the Columbia Hills. J. Geophys. Res. 111, E02S13,
752 doi:10.1029/2005JE002584.

753

754 Morris, R.V. et al., 2006b. Mössbauer mineralogy of rock, soil, and dust at Meridiani
755 Planum, Mars: Opportunity's journey across sulfate-rich outcrop, basaltic sand and dust,
756 and hematite lag deposits. J. Geophys. Res. 111, E12S15, doi:10.1029/2006JE002791.

757

758 Murchie, S. et al., 2007. Compact Reconnaissance Imaging Spectrometer for Mars
759 (CRISM) on Mars Reconnaissance Orbiter (MRO). J. Geophys. Res. 112, E05S03,
760 doi:10.1029/2006JE002682.

761

762 Murchie, S.L. et al., 2009. A synthesis of Martian aqueous mineralogy after 1 Mars year
763 of observations from the Mars Reconnaissance Orbiter. J. Geophys. Res. 114, E00D06,
764 doi:10.1029/2009JE003342.

765

766 Murray, R.W., Miller, D. J., Kryc, K.A., 2000. Analysis of Major and Trace Elements in
767 Rocks, Sediments, and Interstitial Waters by Inductively Coupled Plasma-Atomic
768 Emission Spectrometry (ICP-AES), ODP Tech. Note 29, doi:10.2973/odp.tn.29.2000.

769

770 Mustard, J.F., Pieters, C.M., 1987. Quantitative abundance estimates from bidirectional
771 reflectance measurements. J. Geophys. Res. 92, E617–E626,
772 doi:10.1029/JB092iB04p0E617.
773
774 Mustard. J.F. et al., 2008. Hydrated silicate minerals on Mars observed by the Mars
775 Reconnaissance Orbiter CRISM instrument. Nature 454, 305-309,
776 doi:10.1038/nature07097.
777
778 Navarre-Sitchler, A., Steefel, C.I., Yang, L., Tomutsa, L., Brantley, S.L., 2009. Evolution
779 of porosity and diffusivity associated with chemical weathering of a basalt clast. J.
780 Geophys. Res. 114, F02016, doi:10.1029/2008JF001060.
781
782 Nesbitt, H. W., Young, G. M., 1982. Early Proterozoic climates and plate motions
783 inferred from major element chemistry of lutites. Nature 299, 715-717,
784 doi:10.1038/299715a0.
785
786 Nesbitt, H. W., R. E. Wilson, 1992. Recent chemical weathering of basalts. AJS 292,
787 740-777, doi:10.2475/ajs.292.10.740.
788
789 Ravel, B., 2009. Athena User's Guide. Version 1.5. Downloaded from:
790 http://cars9.uchicago.edu/~ravel/software/doc/Athena/html/athena.pdf
791

792 Rieder, R., Wänke, H., Economou, T., Turkevich, A., 1997. Determination of the
793 chemical composition of Martian soil and rocks: The alpha proton X ray spectrometer. J.
794 Geophys. Res. 102, E2, 4027-4044.
795
796 Ross, P.-S., 2005. Volcanology of the Mawson Formation at Coombs and Allan Hills,
797 South Victoria Land, Antarctica. Ph.D. thesis, Univ. of Otago, Dunedin.
798
799 Salvatore, M.R. et al., 2013a. Development of alteration rinds by oxidative weathering
800 processes in Beacon Valley, Antarctica, and implications for Mars. Geochim.
801 Cosmochim. Acta 115, 137-161, doi:10.1016/j.gca.2013.04.002.
802
803 Salvatore, M.R., Mustard, J.F., Head III, J.W., Marchant, D.R., Wyatt, M.B., 2013b.
804 Characterization of spectral and geochemical variability within the Ferrar Dolerite of the
805 McMurdo Dry Valleys, Antarctica: weathering, alteration, and magmatic processes.
806 Antarctic Science 26, 49-68, doi:10.1017/S0954102013000254.
807
808 Stroncik, N.A., Schmincke, H.-U., 2002. Palagonite – a review. Int. J. Earth Sci. 91, 680-
809 697, doi:10.1007/s00531-001-0238-7.
810
811 Taylor, S.R., 1989. Growth of planetary crusts. Tectonophysics 161, 147-156,
812 doi:10.1016/0040-1951(89)90151-0.
813

814 Thomson, B.J., Hurowitz, J.A., Baker, L.L., Bridges, N.T., Lennon, A.M., Paulsen, G.,
815 Zacny, K., 2014. The effects of weathering on the strength and chemistry of Columbia
816 River Basalts and their implications for Mars Exploration Rover Rock Abrasion Tool
817 (RAT) results. Earth Planetary Sci. Lett. 400, 130-144, doi:10.1016/j.epsl.2014.05.012.
818
819 Van Gorp, B. et al., 2014. Ultra-compact imaging spectrometer for remote, in situ, and
820 microscopic planetary mineralogy. J. App. Rem. Sens. 8, 084988,
821 doi:10.1117/1.JRS.8.084988
822
823 Vaniman, D.T. et al., 2014. Mineralogy of a Mudstone at Yellowknife Bay, Gale Crater,
824 Mars. Science 343, 6169, doi:10.1126/science.1243480.
825
826 White, E.H., McKinstry, H.A., 1966. Chemical effect on X-ray absorption-edge fine
827 structure. Advances in X-ray Analysis 9, 376–392, doi:10.1007/978-1-4684-7633-0_34.
828
829 Wilke, M., Farges, F., Petit, P.-E., Brown Jr., G.E., Martin, F., 2001. Oxidation state and
830 coordination of Fe in minerals: An Fe K-XANES spectroscopic study. American
831 Mineralogist 86, 714-730.
832
833 Wilson, S.A., 1997a, The collection, preparation, and testing of USGS reference material
834 BCR-2, Columbia River, Basalt: U.S. Geological Survey Open-File Report 98-xxx.
835

836 Wilson, S.A., 1997b, Data compilation for USGS reference material BHVO-2, Hawaiian
837 Basalt: U.S. Geological Survey Open-File Report.
838
839 Wiseman, S.M. et al., 2008. Phyllosilicate and sulfate-hematite deposits within Miyamoto
840 crater in southern Sinus Meridiani, Mars. Geophys. Res. Lett. 35, L19204,
841 doi:10.1029/2008GL035363.
842
843 Zolotov, M.Y., Mironenko, M.V., 2014. Massive Sulfate Deposits on Mars could be
844 Remobilized Noachian Salts. In: 45th Lunar and Planetary Science Conference, Abstract
845 #2876.